Role of Plasma in Femtosecond Laser Pulse Propagation

Vladimir Mezentsev[*], Mykhaylo Dubov[*],
Jovana S. Petrovic[*], Ian Bennion[*],
Jürgen Dreher[†] and Rainer Grauer[†]

[*]*Photonics Research Group, Aston University, Birmingham B4 7ET, United Kingdom*
[†]*Theoretische Physik I, Ruhr-Universität Bochum, D-44780 Bochum, Germany*

Abstract. This paper describes physics of nonlinear ultra-short laser pulse propagation affected by plasma created by the pulse itself. Major applications are also discussed. Nonlinear propagation of the femtosecond laser pulses in gaseous and solid transparent dielectric media is a fundamental physical phenomenon in a wide range of important applications such as laser lidars, laser micro-machining (ablation) and microfabrication etc. These applications require very high intensity of the laser field, typically 10^{13}–10^{15} TW/cm2. Such high intensity leads to significant ionisation and creation of electron-ion or electron-hole plasma. The presence of plasma results into significant multiphoton and plasma absorption and plasma defocusing. Consequently, the propagation effects appear extremely complex and result from competitive counteraction of the above listed effects and Kerr effect, diffraction and dispersion. The theoretical models used for consistent description of laser-plasma interaction during femtosecond laser pulse propagation are derived and discussed. It turns out that the strongly nonlinear effects such self-focusing followed by the pulse splitting are essential. These phenomena feature extremely complex dynamics of both the electromagnetic field and plasma density with different spatio-temporal structures evolving at the same time. Some numerical approaches capable to handle all these complications are also discussed.

INTRODUCTION

The main objective of this paper is to outline the role of plasma created during the course of propagation of the intense femtosecond (fs) laser pulse. To be more specific, the applications of this phenomenon in fs microfabrication used as an example. Direct inscription of the complex microstructures in refractive materials by means of intense femtosecond radiation is one of the novel enabling technologies in modern photonics. This technology implies that pre-focused femtosecond light pulses produce phase transitions and create domains with a modified refractive index. Nonlinear propagation of femtosecond intense laser pulses in dielectrics exhibits a wide range of fascinating phenomena including conical emission[1], X-waves[2], self-reconstruction[3], self-healing[2] light filaments plasma breakdown[4]. Proof of principle experiments of the potential of fs inscription for microfabrication of photonic structures was demonstrated almost a decade ago[5]. It has now become a very promising method of microfabrication[6, 7, 8]. Other interesting applications aim to achieve the longest possible self-guiding filaments to de-

liver the energy through the bulk of material[9].
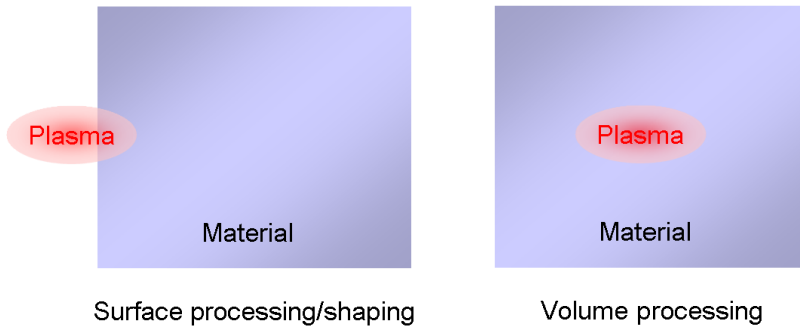
FIGURE 1. Plasma assisted material processing is usually associated with surface treated with plasma (left). We aim internal processing in the bulk of the material with the plasma created by the high power laser pulse

Experimental setup for volume plasma processing is shown in Fig. 2. Intense laser pulse is focused under the surface of the planar sample typically made of fused silica.

Self-focusing of the intense laser pulse is a key physical phenomenon leading to a multi-photon ionization at its final stage. In fact the very formation of plasma filaments limits the catastrophic damage due to defocusing and multi-photon absorption. Eventually, the thermalization and recombination of the plasma filament leads to the modification of medium and a distributed profile of refractive index is produced. The dynamics of the light-induced plasma filaments is extremely complex and defined by many factors. It is an extremely fast process evolving at the very fine spatial scales.
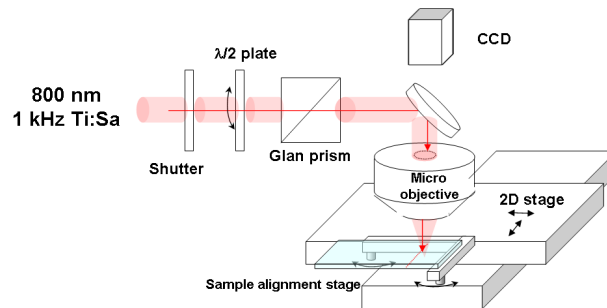
FIGURE 2. Experimental setup for implementation of plasma assisted material processing in the bulk of transparent dielectric

In this paper, we demonstrate and adaptive numerical approach to the detailed study of the evolution of plasma filaments and the role of pulse and media parameters on the shape of resulting filaments. We consider a geometry in which an incident Gaussian input field is focused through a lens into the planar silica sample sample.

170

PLASMA PARAMETERS

This section describes a set of typical parameters for plasma generated by the femtosecond pulse. We consider a couple of limiting factors which define the range of plasma concentration and temperature. One important limitation can be defined from the matching condition between the laser frequency f_e and plasma frequency $f_p = \omega_p/2\pi = (2\pi)^{-1}(\rho e^2/\varepsilon_0 m_e)^{1/2}$ where ρ is an electron concentration. The condition $f_e = f_p$ defines the critical (breakdown) density of plasma $\rho_{BD} = \varepsilon_0 m_e e^{-2} \omega^2$. This is a resonant condition for conversion of electromagnetic wave into plasma waves. It gives a breakdown electron density for a given laser frequency. Typical region of operation parameters is shown in Fig. 3
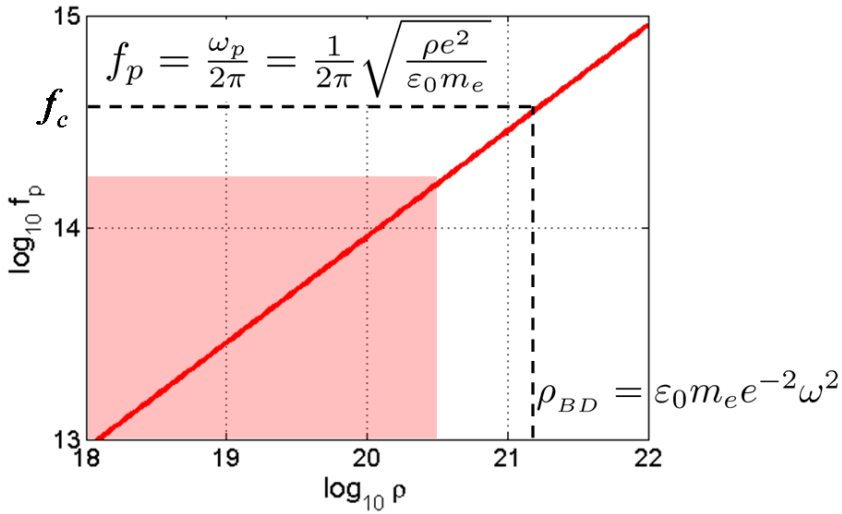
FIGURE 3. Matching of plasma frequency and laser frequency resulting in breakdown condition.

The plasma temperature can be estimated from the analysis of the electron oscillations in high frequency electromagnetic field. Then average kinetic energy can be expressed as

$$K = \left\langle \frac{e^2 \mathscr{E}(t)^2}{4 m_e \omega^2} \right\rangle_t = 9.3 \times 10^{-14} I \lambda^2 \, ,$$

where e and m_e are electron charge and mass respectively, $\mathscr{E}$ is an envelope amplitude of the electric field and I is its intensity, omega is a carrier angular frequency of the electromagnetic wave, and λ is its wavelength. The numerical expression in the right hand side gives a value of the kinetic value in eV provided that intensity is given in W/cm^2 and the wavelength is given in microns. Typical values of electron temperatures versus laser intensity are summarized in Table 1.

Both plasma concentration and temperature characterize a femtosecond laser produced plasma as shown in Fig. 4 in comparison with other types of plasmas.

171

TABLE 1. Average electron energy versus light intensity for typical focusing conditions

Intensity, W/cm^2	10^{13}	10^{14}	10^{15}
Electron energy, eV	0.01	1	100
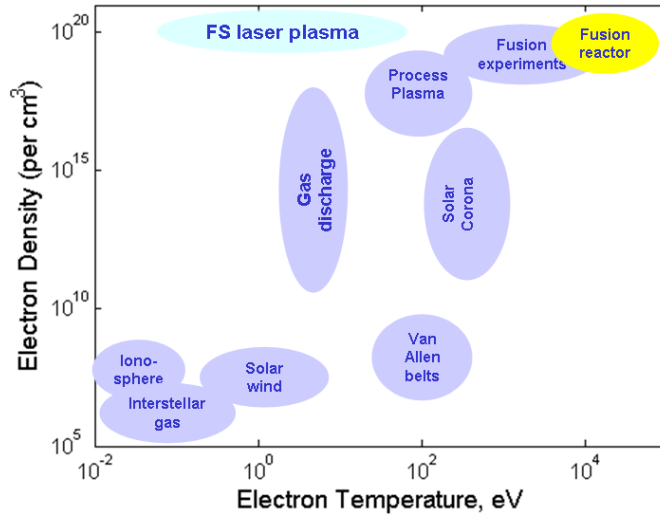
FIGURE 4. Plasma parameters typical for femtosecond laser pulse propagation

THEORETICAL MODEL

Equations

This section describes a theoretical model used for femtosecond pulse propagation in dielectrics. Electromagnetic wave is described by a set of Maxwell equations

$$\nabla \times \mathbf{E} = -\frac{\partial B}{\partial t}$$
$$\nabla \times H = \frac{\partial D}{\partial t} + J$$
$$D = \varepsilon E \; ; \quad B = \mu H \; ,$$

where J is an electron current density.

Description of plasma is based on relaxation dynamics of the electrons driven by the electromagnetic wave. The major source of plasma in strong electromagnetic field is

172

multi-photon and avalanche ionization to be included in the continuity equation.

$$\frac{d\mathbf{v_e}}{dt} = -\tau_c^{-1}\mathbf{v_e} - \frac{e}{m_e}e\mathbf{E}$$

$$\mathbf{J} = -e\rho\mathbf{v_e}$$

$$\frac{d\rho}{dt} = ionization\ sources\ ,$$

where τ_c is the shortest collision time. Envelope approximation can be used to describe quasi-monochromatic paraxial evolution

$$\mathbf{E}(\mathbf{r}_\perp,z,t) = \hat{\mathbf{y}}\mathscr{E}(\mathbf{r}_\perp,z,t)\exp\left[i(kz - \omega t)\right]$$

$$\frac{\partial}{\partial z} = ik + \frac{\partial}{\partial z}\ ;\ \frac{\partial}{\partial t} = -i\omega + \frac{\partial}{\partial t}$$

Finally, Kerr nonlinearity must be taken into account for strong laser field $n = \sqrt{\varepsilon} = n_0 + n_2|\mathscr{E}|^2$. Such approach was originally suggested by Feit and Fleck [14] and later developed into fairly complex models, see e.g. Refs.[15, 16, 17, 9, 18, 19, 20, 21] For the purposes of this paper, a simplified model is used, essentially similar to that described by Feng et al.[10]:

$$i\mathscr{E}_z + \frac{1}{2k}\Delta_\perp\mathscr{E} - \frac{k''}{2}\frac{\partial^2\mathscr{E}}{\partial t^2} + k_0 n_2|\mathscr{E}|^2\mathscr{E} = -\frac{i\sigma}{2}(1 + i\omega\tau)\rho\mathscr{E} - i\frac{\beta^{(K)}}{2}|\mathscr{E}|^{2(K-1)}\mathscr{E} \quad (1)$$

$$\frac{\partial\rho}{\partial t} = \frac{1}{n_b^2}\frac{\sigma_{bs}}{E_g}\rho|\mathscr{E}|^2 + \frac{\beta^{(K)}}{K\hbar\omega}|\mathscr{E}|^{2K} \quad (2)$$

The terms on the left-hand side of Eq.(1) describe effects of beam diffraction, group velocity dispersion (GVD), and Kerr nonlinearity. The latter is responsible for a catastrophic self-focusing which is limited by the effects described by terms on the right-hand side of Eq.(1), namely plasma absorption and multi-photon absorption. In Eq.(1) the laser beam propagation along the z axis is assumed and this equation is essentially a reduced paraxial approximation of the wave equation for the complex electric field envelope $\mathscr{E}$ with a carrier frequency ω in the moving frame of coordinates. Here $k = n_b k_0 = n_b \omega/c$ is the propagation vector, $k'' = \partial^2 k(\omega)/\partial\omega^2$ is the GVD parameter, $n_b(\omega)$ is a linear refractive index of the bulk medium, n_2 is the nonlinear coefficient describing nonlinear self-modulation (Kerr effect) such that $n_2|\mathscr{E}|^2$ is a nonlinear contribution to the refractive index, σ_{bs} is the cross section for inverse Bremsstrallung, τ is the electron relaxation time, E_g is the ionization energy, and the quantity $\beta^{(K)}$ controls the K–photon absorption. Equation (2) implements the Drude model for electron-hole plasma in the bulk of silica and describes the evolution of the electron density ρ. The first term on the right-hand side is responsible for the avalanche impact ionization and the second term — for the ionization resulting from MPA. Equation (2) is suitable for description of the sub–picosecond laser pulses when plasma diffusion is negligible. Here, the wave equation describing the evolution of the focused optical beam in the form of NLSE (left-hand terms in Eq.(1)) which is extended to include plasma generation,

173

pulse-Űplasma interaction, and MPA (terms on the right-hand of Eq.(1). Group velocity dispersion included in Eq.(1) has been shown to lead to pulse splitting and to arrest the collapse [22, 23, 24, 25, 26, 13].

Equations Eqs(1,2) were used for numerical modeling of the plasma formation using adaptive mesh approach described below. We use a simplified version of the widely accepted model of the nonlinear propagation of the laser pulse as it was formulated in Ref.[10]. It is essentially a nonlinear Schrödinger equation (NLSE) coupled with an equation describing the plasma generation. This basic model describes effects of self-focusing, multiphoton absorption (MPA), and group velocity dispersion (GVD). Pure NLSE is a generic model which ultimately appears in consistent description of envelope amplitude of the nonlinear wave packets. It is widely used to describe fs light propagation[11] and has been extensively studied. One of the most striking features of the NLSE is catastrophic self-focusing or beam collapse which means a formation of a singularity in finite propagation length[12]. Beam collapse happens in the framework stationary NLSE if the pulse power exceeds a certain critical value. Formally, the on-axis intensity achieves an infinitely high value at some critical propagation length. However, in the extended physical models which account for dispersion and nonlinear absorption a formation of singularity is arrested[13]. The nonlinear evolution of the collapsing beam with the presence of the arresting effects is extremely rich. Mathematically it poses a stiff multidimensional evolution problem. Straightforward numerical modeling of such problems is a very difficult challenge due to the multiscale nature of underlying physical phenomena. In this paper, we address an intrinsic stiffness of the mathematical problem by introducing a hierarchy of the adaptively refined grids which are dynamically adjusted for proper resolution of the fine spatial structures and temporal features of the beam. We report on the development of a portable computational framework for the parallel, mesh-adaptive solution of system of a 3D parabolic wave equation for envelope amplitude of electromagnetic field coupled with the rate equation for plasma density. Local mesh refinement is realized by the recursive bisection of grid blocks along each spatial and temporal dimensions. Implemented numerical schemes include standard finite-difference and spectral methods. Non-adaptive solver has also been implemented for back-to-back accuracy tests and performance profiling. Parallel execution is achieved through a configurable hybrid of POSIX-multi-threading and MPI-distribution with dynamic load balancing.

Physical parameters

In all our simulations the Gaussian initial condition:

$$\mathscr{E}(z=0,r,t) = \sqrt{\frac{2P_{in}}{\pi r_0^2}} \exp\left(-\frac{r^2}{r_0^2} - \frac{ikr^2}{2f} - \frac{t^2}{t_p^2}\right) , \qquad (3)$$

where r_0 is the waist of the incident beam, t_p defines the conventionally defined pulsewidth $t_{FWHM} = \sqrt{2\ln 2}t_p \approx 1.177t_p$, and f is a focal length of the objective lens.

For all our simulations a fixed single values of $r_0 = 2.5$ mm and $t_p = 60$ fs was used. This fixed pulsewidth corresponds to the critical energy of 116 nJ for a critical power

$P_{cr} = \lambda_0^2/2\pi n_b n_2 \approx 2.3$ MW in fused silica with $n_b = 1.453$ being the linear refraction index and $n_2 = 3.2 \times 10^{-16}$ cm^2/W the nonlinear refraction index. Critical power is proven to be a crucial parameter to determine the evolution of the collapsing beam. We assume the laser wavelength λ_0 to be 800 nm and the focusing lens to have $f = 40$ mm.

The other parameters for fused silica, used in simulations are described below. GVD coefficient $k'' = 361$ fs^2/cm, inverse Bremsstrahlung cross section $\sigma_{bs} = 2.78 \times 10^{-18}$ cm^2. Multiphoton absorption coefficient can be expressed as $\beta^{(K)} \hbar \omega \sigma_K \rho_{at}$, whith $\rho_{at} = 2.1 \times 10^{22}$ atoms/cm^3 being a material concentration and $\sigma_K = 1.3 \times 10{-55}$ cm^{2K}/W^K/s. We assume five–photon ionization with $K = 5$ and $E_g = 7.6$ eV in fused silica.

The quation (2) can be expressed as

$$\frac{\partial}{\partial t} \frac{\rho}{\rho_{BD}} = \frac{1}{n_b^2} \frac{\sigma_{bs}}{E_g} \frac{\rho}{\rho_{BD}} |\mathcal{E}|^2 + \left(\frac{|\mathcal{E}|^2}{I_{MPA}} \right)^K \tag{4}$$

where

$$I_{MPA} = \left(\frac{K \hbar \omega \rho_{BD}}{\beta^{(K)}} \right)^{1/K} \tag{5}$$

is defined to be an MPA threshold as the plasma ionization rate becomes very steep when the intensity I exceeds I_{MPA}. $\rho_{BD} = 1.7 \times 10^{21}$ is a plasma breakdown density. Being important physical thresholds, both I_{MPA} and ρ_{BD} were used in a very useful normalization of physical variables to dimensionless ones for performing simulations. The choice of normalization is irrelevant to discuss as all the parameters and fields throughout this paper are produced with their physical values.

ADAPTIVE NUMERICAL METHOD

The principle of adaptive mesh refinement is rather simple. Starting with one grid of given resolution (in most of our 3D configurations we currently chose 512×64×64 mesh points) called master grid, the partial differential equations (1-2) are solved with a scheme summarized below. After a certain number of steps along propagation axis z, it is checked whether the local numerical resolution is still sufficient on the entire grid. If it is detected that finer grid is locally needed, a refinement is carried out and a child grid is created using the interface with a parent grid as a new boundary. In order to prepare for it, the points where the error of discretization exceeds a given value are marked on the grid. In addition to these grid points, adjacent ones are included. These marked points of insufficient numerical resolution have to be covered with rectangular grids of finer resolution as efficiently as possible. Our algorithm for this purpose is very similar to the one used by Berger and Colella[27], and it was described in detail by Friedel et al.[28]. On the child grids, the spatial discretization length and the time step are reduced by a certain refinement factor. The new grids are filled with data obtained by interpolation from the preceding parent (coarser) level. The integration advances on both the parent and the child levels until the local resolution becomes insufficient again. The rebuilding of the grid hierarchy starting with the current level and proceeding on all subsequent levels begins when the above-mentioned threshold for the error is locally exceeded,

175

e.g., if the domains of high intensity have left the finer grids, or if local gradients have developed, such that the prescribed accuracy is not guaranteed. The points of insufficient numerical resolution are collected on all grids of each level. On the basis of the resulting list of these points, new grids are generated. After assuring that the newly generated grids are properly embedded in their parent grids, interpolated data are filled in. If data existed on grids of the same level before the regridding, these are substituted to the interpolated data from the parents grids.
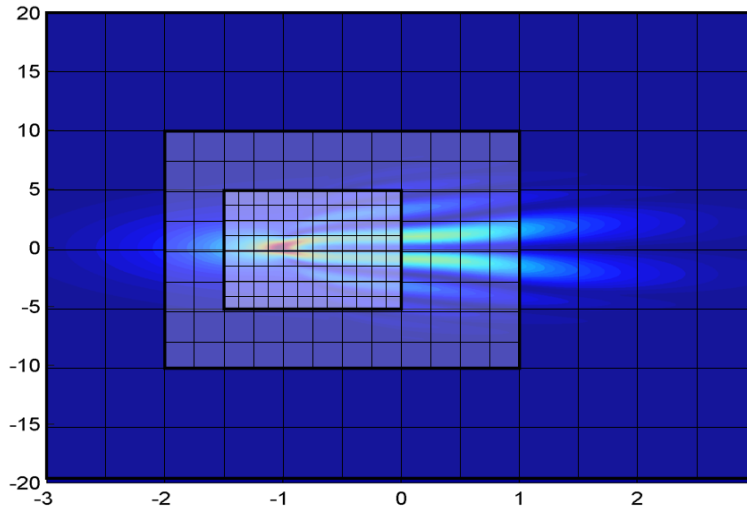
FIGURE 5. Principle of adaptive mesh refinement. Dynamically created child meshes adaptively adjusted to form a hierarchy of meshes for resolving finest details (refining). Fine meshes are removed when fine pattern disappears (coarsening).

Solution of the model described in Introduction in the outlined framework requires selecting an appropriate numerical integration scheme. It turned out that the optimal performance can be achieved by using a different scheme on the refined levels than on the base level, when taking into account that arbitrary mesh sizes on the refined levels occurred. On the base level, we applied an operator–splitting method which is second–order accurate in z. Radial diffraction term in the Laplacian operator of Eq.(1) is integrated by means of Crank–Nicholson scheme with zero boundary condition at the maximum radius. Both the angular term of the transverse diffraction operator and the dispersion operator are diagonal in Fourier space thus Fast Fourier Transform was utilized for numerical integration of these terms. It is worth noting that neither periodic or zero global boundary conditions both in transverse space and time do not impose a significant restriction on the problem considered, because the localized wave-packets vanish at the boundaries during the entire process of focusing and defocusing after the pulse passes the focal domain. On the refined meshes we apply a semi-implicit scheme of Crank-Nicholson type, which was used by, e.g., Pietsch et al.[29] and also utilized in a previous modelling on NLSE with normal dispersion[13].

It is important to comment on the refinement criterion. We calculate the discretized equations based on the actual grid spacing and twice the grid spacing. When the differ-

176

ence exceeds a given threshold, those mesh points are marked under-resolved and are subject to refinement. The threshold value conditioning the refinement was determined such that a sufficient resolution was guaranteed during the evolution along the propagation axis z. The length of the integration step Δz was dynamically adapted to ensure that at all times the i) Courant–Friedrich–Levy condition was met to enforce the numerical stability and the iterative method converged at a prescribed minimal rate and ii) the maximal relative increment of both the amplitude and the nonlinear phase was always kept less than a prescribed limit, usually 1%.

The implementation of the adaptive mesh refinement strategy described above is done in C++. We make use of a non-adaptive solver described above for handling the master grid. This solver was also used for benchmarking and back-to-back accuracy testing of adaptive solver. Handling of the data structures is separated from the problem under consideration. Therefore, it is relatively easy to use the code for other types of problems including various generalizations of the system Eqs.(1-2). Since on each grid the advance along z and the Helmholtz-type equation can be solved independently and the number of grids supersedes the number of processors available, parallelization is highly efficient.

NONLINEAR DYNAMICS

There are two distinct typical setups related to the focusing geometry. If the goal is to produce the longest possible filament, then the loose focusing and small spot size are required [31, 9, 2]. However in the microfabrication context the opposite goal is usually desirable. The focused spot is often required to be as small as possible and the absorbed energy is needed to be within a narrow window between the thresholds of inscription and damage. This is an extremely difficult challenge because of the huge difference in spatial and temporal scales of the incident laser beam and fine features of light and plasma patterns in the vicinity of the focal point. The adaptive procedure described above allows for accurate treatment of multiscale evolution which results in stationary (in the framework of the model considered) distribution of plasma. The mechanisms of eventual plasma recombination and subsequent relaxation of the medium are extremely complex. For example, the latter can be described as a sophisticated 3D thermo-elasto-plastic processes[32]. The purpose of the present work is to find an accurate spatial distribution of plasma needed for such or similar subsequent analysis. Typical asymptotic plasma density profiles for different initial pulse energies are shown energies are shown in Figure 7. Density plots of plasma concentrations are shown in one transverse and one propagation coordinates. It shows that subcritical evolution ($P_{in} < P_{cr}$)leads to a smooth plasma cloud without visible fine structure. This regime is probably the most attractive from the microfabrication viewpoint because it is characterized by the smooth subcritical evolution of the peak intensity. Larger energies lead to development of the pronounced periodic fringes which result from the relaxation oscillations of a collapsing beam after the collapse is arrested by the multiphoton absorption.

ρ/ρ_{BD} I/I_{MPA}

39.934

39.977

39.991

40.005
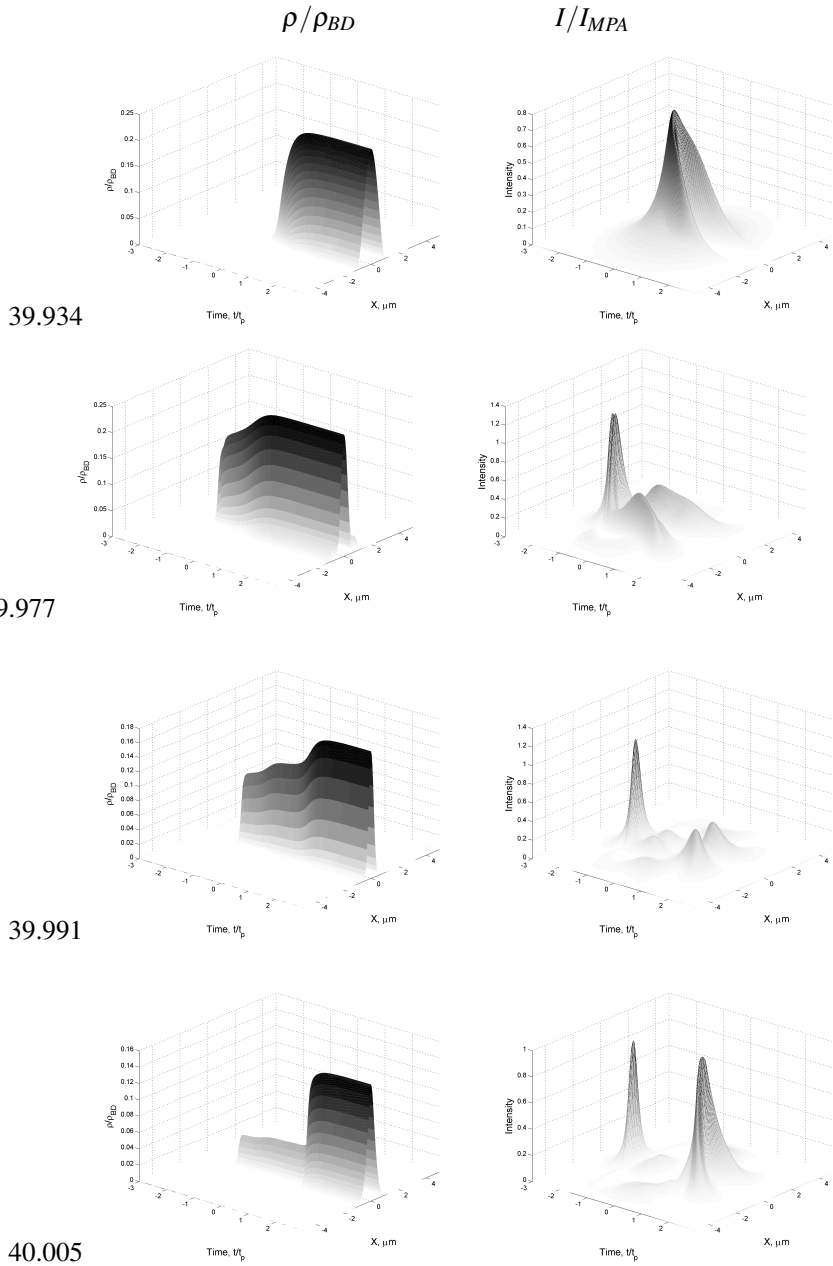
FIGURE 6. Dynamics of the intensity and the plasma density at different positions along axis *z*.

178

Nontrivial complex light and plasma dynamics and formation of interesting light patterns are illustrated by Figure 6. Snapshots of the beam intensity profile in transverse space and time are presented at different points along the propagation axis in the vicinity of the focal point for supercritical case $P_{in} > P_{cr}$. Originally, an intensity profile forms a distinct crescent in $x - t$ plane. It is then evolved so that the shoulders of this crescent split from the front of the pulse and form a pair of satellite pulses which rise being fed by a contracting beam. This pair is eventually coalesce to form a secondary crescent pulse following the remains of the front pulse. Then this scenario repeats for the newborn crescent pulse which even has the same amplitude just under the MPA threshold. A cascade of such crescents result in periodic fringes of plasma density until finally significant fraction of the original pulse energy is absorbed.

The most important result of the intense laser propagation is creation of the cloud of plasma due to ionization. The distribution of electrons can be found as

$$\rho(\mathbf{r}, z) = \int_{-\infty}^{\infty} \left[\frac{1}{n_b^2} \frac{\sigma}{E_g} \rho |\mathscr{E}(\mathbf{r}, z, t)|^2 + \frac{\beta^{(K)}}{K\hbar\omega} |\mathscr{E}(\mathbf{r}, z, t)|^{2K} \right] dt \ .$$

Typical stationary plasma profiles are shown in Fig. 7.
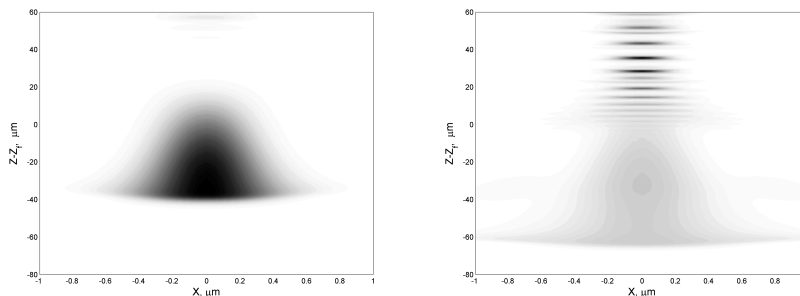
FIGURE 7. Contours of the plasma density at infinite time after electric field is vanished for different energies: subcritical (a) and supercritical (b).

CONCLUSION

It is shown that the dynamics of creation of plasma filaments is a crucial phenomenon in propagation of femtosecond laser pulses in dielectrics. Detailed adaptive numerical modeling of fine dynamics in the vicinity of the focal point reveals an extremely complex behavior of the focused light coupled to generated plasma.

ACKNOWLEDGMENTS

REFERENCES

1. O. G. Kosareva, V. P. Kandidov, A. Brodeur, C. Y. Chien, and S. L. Chin, *Opt. Lett.* **22**, 1332–1334 (1997).
2. M. Kolesik, E. M. Wright, and J. Moloney, *Phys. Rev. Lett.* **92**, 253901 (2004).
3. A. Dubietis, E. Kucinskas, G. Tamosauskas, E. Gaizauskas, M. A. Porras, and P. D. Trapani, *Opt. Lett.* **29**, 2893–2895 (2004).
4. C. W. Carr, M. D. Feit, A. M. Rubenchik, P. D. Mange, S. O. Kucheyev, M. D. Shirk, H. B. Radousky, and S. G. Demos, *Opt. Lett.* **30**, 661–663 (2005).
5. K. M. Davis, K. Miura, N. Sugimoto, and K. Hirao, *Opt. Letters* **21**, 1729–1731 (1996).
6. C. B. Schaffer, A. Brodeur, J. F. Garcìa, and E. Mazur, *Opt. Lett.* **26**, 93–95 (2001).
7. A. H. Nejadmalayeri, P. R. Herman, J. Burghoff, M. Will, S. Nolte, and A. Tuennermann, *Opt. Lett.* **30**, 964–966 (2005).
8. A. M. Kowalevicz, V. Sharma, E. P. Ippen, J. G. Fujimoto, and K. Minoshima, *Opt. Lett.* **30**, 1060–1062 (2005).
9. S. Tzortzakis, L. Sudrie, M. Franco, B. Prade, A. Mysyrowicz, A. Couairon, and L. Bergé, *Phys. Rev. Lett.* **21**, 213902 (2001).
10. Q. Feng, J. V. Moloney, A. C. Newell, E. M. Wright, K. Cook, P. K. Kennedy, D. X. Hammer, B. A. Rockwell, and C. R. Thompson, *IEEE Journal of Quantum Electronics* **33**, 127–137 (1997).
11. J. H. Marburger, *Prog. Quantum Electron.* **4**, 35Ű–110 (1975).
12. V. P. S.N. Vlasov, and V. Talanov, *Izv. Vuzov, Radiofizica* **14**, 1353–1364 (1971).
13. K. Germaschewski, R. Grauer, L. Bergé, V. K. Mezentsev, and J. J. Rasmussen, *Physica D* **151**, 175–198 (2001).
14. M. D. Feit, and J. A. Fleck, *Appl. Phys. Lett.* **24**, 169–Ű172 (1974).
15. T. Brabec, and F. Krausz, *Phys. Rev. Lett.* **78**, 3282Ű–3285 (1997).
16. J. K. Ranka, and A. L. Gaeta, *Opt. Lett.* **23**, 534–536 (1998).
17. A. L. Gaeta, *Phys. Rev. Lett.* **84**, 3582–3585 (2000).
18. M. Kolesik, J. V. Moloney, and M. Mlejnek, *Phys. Rev. Lett.* **89**, 283902 (2002).
19. S. Tzortzakis, L. Bergé, M. Franco, B. Prade, A. Mysyrowicz, and A. Couairon, *J. Opt. Soc. Am. B* **19**, 1117–1129 (2002).
20. M. Kolesik, G. Katona, J. Moloney, and E.M.Wright, *Phys. Rev. Lett.* **91**, 043905 (2003).
21. R. Nuter, S. Skupin, and L. Bergé, *Opt. Lett* **30**, 917–919 (2005).
22. N. A. Zharova, A. G. Litvak, T. A. Petrova, A. M. Sergeev, and A. D. Yunakovskii, *PisŠma Zh. Eksp. Teor. Fiz. (JETP Lett.)* **44**, 12–15 (1986).
23. P. Chernev, and V. Petrov, *Opt. Lett.* **17**, 172–Ű174 (1992).
24. J. E. Rothenberg, *Opt. Lett.* **17**, 583–Ű585 (1992).
25. G. G. Luther, J. V. Moloney, A. C. Newell, and E. M. Wright, *Opt. Lett.* **19**, 862–864 (1994).
26. G. G. Luther, A. C. Newell, and J. V. Moloney, *Physica D* **74**, 59–73 (1994).
27. M. J. Berger, and P. Colella, *J. Comp. Phys.* **82**, 64–84 (1989).
28. H. Friedel, R. Grauer, and C. Marliani, *J. Comp. Phys.* **134**, 190–198 (1997).
29. H. Pietsch, E. Laedke, and K.-H. Spatschek, *Phys. Rev. E* **47**, 1977–1995 (1993).
30. W. Hackbusch, *Iterative Solution of Large Sparse Systems of Equations*, Springer, New York, 1994.
31. A. Dubietis, G. Tamoauskas, I. Diomin, and A. Varanaviiuset, *Opt. Lett* **28**, 1269–1271 (2003).
32. X. Zhang, X. Xu, and A. Rubenchik, *Appl. Phys. A* **79**, 945Ű–948 (2004).